

High-Fidelity Extraction of Neural Network Models

Matthew Jagielski[†], Nicholas Carlini*, David Berthelot*, Alex Kurakin*, Nicolas Papernot*

*Google Research, [†]Northeastern University

Abstract—Model extraction allows an adversary to steal a copy of a remotely deployed machine learning model given access to its predictions. Adversaries are motivated to mount such attacks for a variety of reasons, ranging from reducing their computational costs, to eliminating the need to collect expensive training data, to obtaining a copy of a model in order to find adversarial examples, perform membership inference, or model inversion attacks.

In this paper, we taxonomize the space of model extraction attacks around two objectives: *accuracy*, i.e., performing well on the underlying learning task, and *fidelity*, i.e., matching the predictions of the remote victim classifier on any input.

To extract a high-accuracy model, we develop a learning-based attack which exploits the victim to supervise the training of an extracted model. Through analytical and empirical arguments, we then explain the inherent limitations that prevent any learning-based strategy from extracting a truly high-fidelity model—i.e., extracting a functionally-equivalent model whose predictions are identical to those of the victim model on all possible inputs. Addressing these limitations, we expand on prior work to develop the first practical functionally-equivalent extraction attack for direct extraction (i.e., without training) of a model’s weights.

We perform experiments both on academic datasets and a state-of-the-art image classifier trained with 1 billion proprietary images. In addition to broadening the scope of model extraction research, our work demonstrates the practicality of model extraction attacks against production-grade systems.

I. INTRODUCTION

Machine learning, and neural networks in particular, are widely deployed in industry settings. Models are often deployed as prediction services or otherwise exposed to potential adversaries. Despite this fact, the trained models themselves are often proprietary and are closely guarded.

There are two reasons models are often seen as sensitive. First, they are expensive to obtain. Not only is it expensive to train the final model [1] (e.g., NVIDIA recently trained a model with 8 billion parameters on hardware costing 36 million dollars [2]), performing the work to identify the optimal set of model architecture, training algorithm, and hyper-parameters often eclipses the cost of training the final model. Further, training these models also requires investing in expensive collection process to obtain the training datasets necessary to obtain an accurate classifier [3–6]. Second, there are security [7, 8] and privacy [9, 10] concerns for revealing trained models to potential adversaries.

Concerningly, prior work found that an adversary with query access to a model can steal the model to obtain a copy that largely agrees with the remote victim models [8, 11–16]. These extraction attacks are therefore important to consider.

In this paper, we systematize the space of model extraction around two adversarial objectives: *accuracy* and *fidelity*. Ac-

curacy measures the correctness of predictions made by the extracted model on the test distribution. Fidelity, in contrast, measures the general agreement between the extracted and victim models on any input. Observe that these two objectives are in conflict for imperfect victim models: a high-fidelity extraction should replicate the errors of the victim, whereas a high-accuracy model should instead try to make an accurate prediction. At the high-fidelity limit is *functionally-equivalent* model extraction: the two models agree on all inputs, both on and off the underlying data distribution.

While most prior work considers accuracy [7, 11, 13], we argue that fidelity is often equally important. When using model extraction to mount black-box adversarial example attacks [7], fidelity ensures the attack is more effective because more adversarial examples transfer from the extracted model to the victim. Membership inference [9, 10] benefits from the extracted model closely replicating the confidence of predictions made by the victim. Finally, a functionally-equivalent extraction enables the adversary to inspect whether internal representations reveal unintended attributes of the input—that are statistically uncorrelated with the training objective, enabling the adversary to benefit from overlearning [17].

We design two attacks. First, a *learning-based attack*, which uses the victim to generate labels for training the extracted model. While existing techniques already achieve high accuracy, our attacks are over 16x more query-efficient and scale to large models. We perform experiments that surface inherent limitations of learning-based extraction attacks and argue that learning-based strategies are ill-suited to achieve high-fidelity extraction. Then, the first practical *functionally-equivalent attack*, which directly recovers a two-layer neural network’s weights exactly given access to double-precision model inference. Compared to prior work, which required a high-precision power side-channel [18] or access to model gradients [19], our attack only requires input-output access to the model, while simultaneously scaling to larger networks.

We make the following contributions:

- We taxonomize the space of model extraction attacks by exploring the objective of *accuracy* and *fidelity*.
- We significantly improve the query efficiency of learning-based attacks and make them practical for millions-of-parameter models trained on billions of images.
- We achieve high-fidelity extraction by developing the first practical functionally-equivalent model extraction attack.
- We mix the proposed methods to obtain a hybrid method which improves both accuracy and fidelity extraction.
- We discuss mitigation strategies for model extraction.

II. PRELIMINARIES

For $n \in \mathbb{Z}$, we write $[n] = \{1, 2, \dots, n\}$. We consider classifiers with domain $\mathcal{X} \subseteq \mathbb{R}^d$ and range $\mathcal{Y} \subseteq \mathbb{R}^K$; the output of the classifier is a distribution over K class labels. For a classifier f , the class assigned to an input x by f is $\arg \max_{i \in [K]} f(x)_i$. In order to satisfy the constraint that a classifier's output is a distribution, a *softmax* $\sigma(\cdot)$ is typically applied to the output of an arbitrary function $f_L : \mathcal{X} \rightarrow \mathbb{R}^K$:

$$\sigma(f_L(x))_i = \frac{\exp(f_L(x)_i)}{\sum_j \exp(f_L(x)_j)}.$$

We call the function $f_L(\cdot)$ the *logit function* for a classifier f . To convert a class label into a probability vector, it is common to use *one-hot encoding*: for a value $j \in [K]$, the one-hot encoding $OH(j; K)$ is a vector in \mathbb{R}^K with $OH(j; K)_i = \mathbb{1}(i = j)$ —that is, it is 1 only at index j , and 0 elsewhere.

Model extraction concerns reproducing a victim model, or oracle, which we write $\mathcal{O}(\cdot) : \mathcal{X} \rightarrow \mathcal{Y}$. The model extraction adversary will run an extraction algorithm $\mathcal{A}(\mathcal{O})$, which outputs the extracted model $\hat{\mathcal{O}}(\cdot)$. We will sometimes parameterize the oracle (resp. extracted model) as \mathcal{O}_θ (resp. $\hat{\mathcal{O}}_\theta$) to denote that it has model parameters θ —we will omit this when unnecessary or apparent from context.

In this work, we consider $\mathcal{O}(\cdot)$ and $\hat{\mathcal{O}}(\cdot)$ to both be neural networks. A neural network is a sequence of operations—alternatingly applying linear operations and non-linear operations—a pair of linear and non-linear operations is called a *layer*. Each linear operation projects onto some space \mathbb{R}^h —the dimensionality h of this space is referred to as the *width* of the layer. The number of layers is the *depth* of the network. The non-linear operations are typically fixed, while the linear operations have parameters which are learned during training. The function computed by layer i , $f_i(a)$, is therefore computed as $f_i(a) = g_i(A^{(i)}a + B^{(i)})$, where g_i is the i th non-linear function, and $A^{(i)}, B^{(i)}$ are the parameters of layer i ($A^{(i)}$ is the weights, $B^{(i)}$ the biases). A common choice of activation is the rectified linear unit, or ReLU, which sets $\text{ReLU}(x) = \max(0, x)$. Introduced to improve the convergence of optimization when training neural networks, the ReLU activation has established itself as an effective default choice for practitioners [20]. Thus, we consider primarily ReLU networks in this work.

The network structure described here is called *fully connected* because each linear operation “connects” every input node to every output node. In many domains, such as computer vision, this is more structure than necessary. If a neuron learns an edge detector, for example, it only needs to use information in a small region of the input space, not the whole scene. *Convolutional networks* were developed to combat this inefficiency—the linear functions become filters, which are still linear, but are only applied to a small (say 3x3 or 5x5) window of the input. They are applied in turn to every such window using the same weights, making convolutions require much fewer parameters than fully connected networks.

Neural networks are trained by *empirical risk minimization* (ERM). Given a dataset of n samples $\mathcal{D} = \{x_i, y_i\}_{i=1}^n$,

which is a multiset of elements from $\mathcal{X} \times \mathcal{Y}$, training involves minimizing a loss function L on the dataset with respect to the network parameters of the network f . A common loss function is the cross-entropy loss H for a sample (x, y) :

$$H(y, f(x)) = - \sum_{k \in [K]} y_k \log(f(x)_k),$$

where y is the probability (or one-hot) vector for the true class. The cross-entropy loss on the full dataset is then

$$L(\mathcal{D}; f) = \frac{1}{n} \sum_{i=1}^n H(y_i, f(x_i)).$$

The loss is minimized with some form of gradient descent. The most basic optimizer is stochastic gradient descent (SGD). In SGD, gradients of the model parameters θ are computed over a batch B containing b samples, averaged, and scaled by a learning rate η :

$$\theta_{t+1} = \theta_t - \frac{\eta}{b} \sum_{i \in B} \nabla_{\theta} H(y_i, f(x_i)).$$

Other optimizers exist [21–23] which use gradient statistics to reduce the variance of updates.

A less common setting, but one which is important for our work, is when the target values y which are used to train the network are not one-hot values, but are probability vectors output by a different model $g(x)$. When training using the dataset $\mathcal{D}_g = \{x_i, g(x_i)\}_{i=1}^n$, we say the trained model is *distilled* from g , referring to the process of distillation introduced in Hinton *et al.* [24].

III. TAXONOMY OF THREAT MODELS

We now address the spectrum of adversaries interested in extracting neural networks. As illustrated in Table I, we taxonomize the space of possible adversaries around two overarching goals—*theft* and *reconnaissance*. We detail why extraction is not always practically realizable through the analytical construction of models that are impossible to extract, or require a large number of queries to extract. We conclude our threat model with a discussion of how adversarial capabilities (e.g., prior knowledge of the model's architecture or how much information is returned by queries made to the model) affect the strategies an adversary may consider.

A. Adversarial Motivations

Model extraction attacks target the *confidentiality* of a victim model deployed on a remote service. By model, we refer here to both the architecture and its parameters. Architectural details include the learning hypothesis (i.e., neural network in our case) and corresponding details (e.g., number of layers and activation functions for neural networks). Parameter values are the result of training. The adversary may be interested in violating the model's confidentiality for several reasons falling under two broad classes: *theft* and *reconnaissance*.

Generally, the defender went through an expensive process to design the model's architecture and train it to set parameter values. This drives the first class of attacks where *theft*

Attack	Type	Model type	Goal	Query Output
Lowd & Meek [8]	Direct Recovery	Linear models	Functionally Equivalent	Labels
Tramer <i>et al.</i> [11]	(Active) Learning	Linear models, neural networks	Task Accuracy, Fidelity	Probabilities, labels
Tramer <i>et al.</i> [11]	Path finding	Decision trees	Functionally Equivalent	Probabilities, labels
Milli <i>et al.</i> [19] (theoretical)	Direct Recovery	Neural network (2 layer)	Functionally Equivalent	Gradients, logits
Milli <i>et al.</i> [19]	Learning	Linear model, neural network	Task Accuracy	Gradients
Pal <i>et al.</i> [15]	Active learning	Neural network	Fidelity	Probabilities, labels
Chandrasekharan <i>et al.</i> [13]	Active learning	Linear models	Functionally Equivalent	Labels
Copycat CNN [16]	Learning	Convolutional neural network	Task Accuracy, Fidelity	Labels
Papernot <i>et al.</i> [7]	Active learning	Neural network	Fidelity	Labels
CSI NN [25]	Direct Recovery	Neural network	Functionally Equivalent	Power Side Channel
Knockoff Nets [12]	Learning	Neural network	Task Accuracy	Probabilities
Functionally equivalent (this work)	Direct Recovery	Neural network (2 layer)	Functionally Equivalent	Probabilities, logits
Efficient learning (this work)	Learning	Neural network	Task Accuracy, Fidelity	Probabilities

TABLE I
EXISTING MODEL EXTRACTION ATTACKS

adversaries are motivated by economic incentives. Here, the model can be viewed as intellectual property that the adversary is trying to steal. A line of work has in fact referred to this as “model stealing” [11].

In the latter class of attacks, the adversary may be performing *reconnaissance* to later mount attacks targeting other security properties of the learning system: e.g., its integrity with adversarial examples [7], or privacy with training data membership inference [9, 10]. In particular, model extraction enables an adversary previously operating in a black-box threat model to mount attacks against the extracted model in a white-box threat model because the adversary has—by design—access to the extracted model’s parameters. In the limit, an adversary motivated by reconnaissance would expect to extract an *exact* copy of the oracle.

The goal of **exact extraction** is to produce $\hat{\mathcal{O}}_\theta = \mathcal{O}_\theta$ —that is, the model architecture as well as all of its weights should be identical. This definition is presented purely as a strawman—it is the strongest possible attack one could want, but it is fundamentally impossible for many classes of neural networks. Take the example of ReLU networks. It is easy to, given a ReLU network, construct an equivalence class of networks which are indistinguishable from input-output behavior. To do so, we can pick any neuron, and scale its incoming weights and biases by some $c > 0$, and scale its outgoing weights and biases by c^{-1} . Alternatively, for any hidden layer, it is possible to permute its neurons or even add a dead neuron—that is, a neuron whose output is always zero—both of which are unobservable from input-output relationships. From these examples, we can see that exact extraction cannot be done—the best we can do is identify the equivalence class the oracle belongs to.

B. Adversarial Goals

This perspective yields a natural spectrum of realistic adversarial goals characterizing decreasingly precise extractions.

a) Functionally Equivalent Extraction: The goal of functionally equivalent extraction is to construct an $\hat{\mathcal{O}}$ such that $\forall x \in \mathcal{X}$, $\hat{\mathcal{O}}(x) = \mathcal{O}(x)$. This is a tractable weakening of

the exact extraction definition from earlier—it is the hardest possible goal given observation of input-output pairs only. The adversary obtains a member of the equivalence class the oracle belongs to. This extraction enables a number of downstream attacks, including those like overlearning [17]—that involve an inspection of the model’s internal representations, to operate in the white-box threat model.

b) Fidelity Extraction: Given some target distribution \mathcal{D}_F over \mathcal{X} , and goal similarity function $S(p_1, p_2)$, the goal of fidelity extraction is to construct an $\hat{\mathcal{O}}$ that maximizes $\Pr_{x \sim \mathcal{D}_F} [S(\hat{\mathcal{O}}(x), \mathcal{O}(x))]$. In this work, we consider only *label agreement*, where $S(p_1, p_2) = \mathbb{1}(\arg \max(p_1) = \arg \max(p_2))$; we leave exploration of other similarity functions to future work.

A natural distribution of interest \mathcal{D}_F is the data distribution itself—the adversary wants to make sure the mistakes and correct classifications are the same between the two models. A reconnaissance attack for constructing adversarial examples would use as its distribution a perturbed data distribution; mistakes might be more important to the adversary in this setting. Membership inference would use the natural data distribution, including any outliers. These distributions tend to be concentrated on a low-dimension manifold of \mathcal{X} , making fidelity extraction significantly easier than functionally equivalent extraction. Indeed, functionally equivalent extraction achieves a perfect fidelity of 1 on *all distributions* and *all distance functions*.

c) Task Accuracy Extraction: For the true task distribution \mathcal{D}_A over $\mathcal{X} \times \mathcal{Y}$, the goal of task accuracy extraction is to construct an $\hat{\mathcal{O}}$ maximizing $\Pr_{(x,y) \sim \mathcal{D}_A} [\arg \max(\hat{\mathcal{O}}(x)) = y]$. This goal is to match (or exceed) the accuracy of the target model, which is the easiest goal to consider in this taxonomy (because it doesn’t need to match the mistakes of \mathcal{O}).

C. Model Extraction is Hard

Before we consider adversarial capabilities in Section III-D and potential corresponding approaches to model extraction, we must understand how successful we can hope to be. Here,

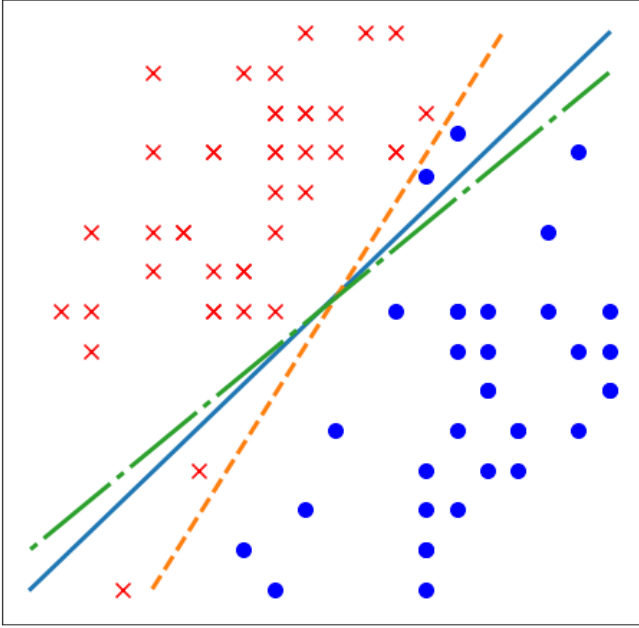


Fig. 1. An illustration of fidelity and accuracy. The solid blue line is the oracle: functionally identical extraction would recover this line precisely. The green dash-dot line achieves perfect label fidelity: it matches the oracle’s predictions on all data. The orange dashed line achieves perfect accuracy: it classifies all points correctly. Fidelity with label agreement on the test distribution and task accuracy extraction differ on points the oracle misclassifies. Note that we used label agreement to measure fidelity. If we had instead measured fidelity as a distance between the oracle and extracted model’s outputs, the green dash-dot line may not achieve perfect fidelity.

we present arguments that will serve to bound our expectations. First, we will identify some limitations of functionally equivalent extraction by constructing networks which can require arbitrarily many queries to extract. Second, we will present another class of networks that cannot be extracted with fidelity without querying an exponential number of times in its depth. We provide intuition in this section and later prove these statements in Appendix A.

1) *Functionally equivalent extraction can require exponentially many queries:* In order to show that functionally equivalent extraction is intractable in the worst case, we provide a construction of a class of neural networks that are hard to extract without making exponentially many queries in the network’s width.

Theorem 1. *There exists a class of width $3k$ and depth 2 neural networks on domain $[0, 1]^d$ with $d \geq c$ that require 256^k queries to extract.*

It is in fact possible to make the value of 256 larger—this particular value reflects an 8-bit pixel value range in image classification domains. The intuition for this theorem is that a width $3k$ network can implement a function that only returns a non-zero value on at most a 256^{-k} fraction of the space. In the worst case, 256^k queries are necessary to find this fraction of the space.

Note that this result assumes the adversary is only allowed

to observe the input-output query behavior of the oracle. If this assumption is broken then functionally equivalent extraction becomes practical. For example, Batina *et al.* [25] perform functionally equivalent extraction by performing a side channel attack (specifically, differential power analysis [26]) on a microprocessor evaluating the neural network.

We also observe in Theorem 2 that, given white-box access to two neural networks, it is NP-hard in general to test if they are functionally equivalent. We do this by embedding a subset sum instance into a neural network, so that it is nonzero only on an input corresponding to a satisfying subset, and 0 elsewhere. Then finding a nonzero location in this network is as hard as finding a satisfying subset.

Theorem 2 (Informal). *Given the weights of two neural networks, testing whether they are functionally equivalent is NP-hard.*

Any attack which can claim to perform functionally equivalent extraction efficiently (both in number of queries used and in running time) must make some assumptions to avoid these pathologies. Later, when we present a functionally equivalent extraction attack for two-layer neural network models, we will be clear how its assumptions allow us to recover the functionally equivalent model.

2) Learning approaches struggle with fidelity extraction:

A final difficulty for model extraction comes from recent work in learnability [27]. Das *et al.* prove that, for deep random networks with input dimension d and depth h , model extraction approaches that can be written as Statistical Query (SQ) learning algorithms require $\exp(O(h))$ samples for distributional extraction. Statistical query algorithms are a restricted form of learning algorithm which only allows access to the data with noisy aggregate statistics; many prevalent learning algorithms, such as (stochastic) gradient descent and PCA, are examples. As a result, most learning-based approaches to model extraction will inherit this inefficiency. A sample-efficient approach therefore must either make assumptions about the model to be extracted (to distinguish it from a deep random network), or must access its dataset in nonuniform ways, avoiding statistical queries.

Theorem 3 (Informal [27]). *Random networks with domain $\{0, 1\}^d$ and range $\{0, 1\}$ and depth h require $\exp(O(h))$ samples to learn in the SQ learning model.*

D. Adversarial Capabilities

Adversaries may have varying levels of prior knowledge about the oracle and the data used to train it. These can be organized into three broad categories—*domain knowledge*, *deployment knowledge*, and *model access*.

1) **Domain Knowledge:** Limiting the adversary’s domain knowledge is a strong assumption, and so adversaries should be assumed to have as much domain knowledge as the oracle’s designer. Domain knowledge characterizes what the adversary knows about the task the model was designed for. For example, if the model is an image classifier, then the model should

predict similarly under standard image data augmentations, such as shifts, rotations, or crops.

In certain cases, the adversary can also be assumed to have access to public pretrained models or public datasets relevant to the task of interest. This is often the case for learning-based model extraction, which we develop in Section IV. We consider an adversary using part of a public dataset of 1.3 million images [4] as unlabeled data to mount an attack against a model trained on a proprietary dataset consisting of 1 billion labeled images [28].

a) Learning-based extraction is hard without natural data: When performing learning-based extractions, we assume that the adversary is able to collect public *unlabeled* data to mount their attack. For a theft-motivated adversary who wishes to steal the oracle for local use, this is a natural assumption—this adversary has data they want to learn the labels of without querying the model. For other adversaries, progress in generative modeling is likely to offer ways to remove this assumption [29]. We leave this to future work because our overarching aim in this paper is to characterize the model extraction attacker space around the notions of accuracy and fidelity. All progress achieved by our approaches is complementary to possible progress in synthetic data generation.

2) Deployment Knowledge: Deployment knowledge characterizes what the adversary knows about the oracle itself. This includes the precise model architecture, training procedure, and the model’s training dataset. The adversary may have access to public artifacts of the oracle—a distilled version of the oracle may be available (such as for OpenAI GPT [30]) or the oracle may be transfer learned from a public pretrained model (as is the case for many image classifiers [31] or language models like BERT [32]).

In addition, the adversary may or may not have access to the feature and label sets. That is, the features that make up the inputs of the model and the classes the model may output. While the latter can generally be inferred by interacting with the model (e.g., making queries and observing the labels predicted by the model), the former is generally more difficult to infer. While our preliminary investigations suggest that these are not limiting assumptions, we leave proper treatment of this aspect to future work.

3) Model Access: Model access characterizes what information the adversary obtains from the oracle. For example, the adversary may have a bound on the number of queries they can make. They may also require different strategies depending on whether queries are answered with:

- *label*: only the label of the most-likely class is revealed.
- *label and score*: in addition to the most-likely label, the confidence score of the model in its prediction for this label is revealed.
- *top-k scores*: the labels and confidence scores for the k classes whose confidence are highest are revealed.
- *scores*: confidence scores for all labels are revealed.
- *logits*: raw logit values for all labels are revealed.

In general, the more access an adversary is given, the more effective they should be in accomplishing their goal. We

instantiate practical attacks under several of these assumptions. We also discuss model access in more details in Section VIII where we detail potential defensive strategies to limit adversarial access to the model effectively while preserving quality of service for legitimate users.

IV. LEARNING-BASED MODEL EXTRACTION

We present our first attack strategy where the victim model serves as a labeling oracle for the adversary. While many attack variants exist [7, 11], they generally stage an iterative interaction between the adversary and the oracle, where the adversary collects labels for a set of points from the oracle and uses them as a training set for the extracted model.

Here, we realistically simulate large-scale model extraction by considering an oracle that was trained on 1 billion Instagram images [28] to obtain (at the time of the experiment) state-of-the-art performance on the standard image classification benchmark, ImageNet [4]. The oracle, with 193 million parameters, obtained 84.2% top-1 accuracy and 97.2% top-5 accuracy on the 1000-class benchmark—we will refer to the model as the “WSL model”, abbreviating the paper title. We give the adversary access to the public ImageNet dataset. The adversary’s goal is to use the WSL model as a labeling oracle to train an ImageNet classifier that performs better than if we trained the model directly on ImageNet. *The attack is successful if access to the WSL model—trained on 1 billion proprietary images inaccessible to the adversary—enables the adversary to extract a model that outperforms a baseline model trained directly with ImageNet labels.*

We consider two variants of the attack: one where the adversary selects 10% of the training set (i.e., about 130,000 points) and the other where the adversary keeps the entire training set (i.e., about 1.3 million points). To put this number in perspective, recall that each image has a dimension of 224x224 pixels, where each pixel color is encoded with three channels, hence bringing the number of model input features to $224 \cdot 224 \cdot 3 = 150,528$ features. Each image belongs to one of 1,000 categories. Although ImageNet data is labeled, we always treat it as unlabeled to simulate a realistic adversary.

A. Fully-supervised model extraction

This first attack is fully supervised. It serves both as an experiment to validate our hypothesis that labels returned by the oracle are more informative than dataset labels, and also as a way for us to compare our subsequent attacks with prior work which employed fully-supervised extraction.

The adversary needs to obtain a label for each of the points it intends to train the extracted model with. The oracle is thus queried to label the adversary’s training points with the oracle’s predictions. The oracle reveals its full prediction vector (i.e., *labels and scores* in the threat model from Section III) when queried. This assumption is challenged later in Section VIII, where we show that the adversary is not significantly weakened when it only has access to the top-5 label predictions and scores.

Readers familiar with knowledge transfer will note that this process follows closely the one of distillation [24]. In fact, one of the innovations of our attack is to simulate¹ the temperature parameter—central to distillation—as a means to control how much weight is placed on the runner-up classes when training our victim model. Specifically, we post-process the oracle’s response $\mathcal{O}(x)$ to form the following training label $\mathcal{O}_T(x)$:

$$\mathcal{O}_T(x)_i = \frac{\mathcal{O}(x)_i^{1/T}}{\sum_j \mathcal{O}(x)_j^{1/T}} \quad (1)$$

The adversary then trains its model to match these labels using the cross-entropy loss. We used $T = 1.5$ in our experiments after a random search. Our experiments use two architectures known to perform well on image classification: ResNet-v2-50 and ResNet-v2-200.

Results. We present results in Table II. For instance, the adversary is able to improve the accuracy of their model by 1.0% for ResNetv2-50 and 1.9% for ResNet_v2_200 after having queried the oracle for 10% of the ImageNet data. Recall that the task has 1,000 labels, making these increases significant. The gains we are able to achieve as an adversary are in line with progress that has been made by the computer vision community on the ImageNet benchmark over the last years, where each year the research community improved the state-of-the-art top-1 accuracy by about a single percent point.²

B. Improving query efficiency with unlabeled data

For adversaries interested in theft, a learning-based strategy should minimize the number of queries required to achieve a given level of accuracy. A natural approach towards this end is to take advantage of advances in label-efficient ML, including active learning [35] and semi-supervised learning [36].

Active learning allows a learner to query the labels of arbitrary points—the goal is to query the best set of points to learn a model with. Semi-supervised learning considers a learner with some labeled data, but much more unlabeled data—the learner seeks to leverage the unlabeled data (without labeling it) to improve performance on the classification task.

The connection between label-efficient learning and learning-based model extraction attacks is not new [11, 13, 15], but has focused on active learning approaches. *We demonstrate that, given the assumption of unlabeled task-specific data, semi-supervised learning is also an effective approach to improving model extraction attacks.* We explore two techniques: the rotation loss [34] and MixMatch [37].

Rotation loss. We leverage the current state-of-the-art semi-supervised learning approach on ImageNet, which augments the model with a *rotation loss* [34]. An extra linear classifier is added on top of the final-layer representation. The goal of this extra function is to predict the rotation applied to an

input—each input is fed in four times per batch, rotated by $\{0^\circ, 90^\circ, 180^\circ, 270^\circ\}$. The classifier should output one-hot encodings $\{OH(0; 4), OH(1; 4), OH(2; 4), OH(3; 4)\}$, respectively, for these rotated images. Then, the loss is written as:

$$L_R(X; f_\theta) = \frac{1}{4N} \sum_{i=0}^N \sum_{j=1}^r H(f_\theta(R_j(x_i)), j)$$

where R_j is the j th rotation, H is cross-entropy loss, and f_θ is the model’s probability outputs for the rotation task. Inputs need not be labeled, hence we compute this loss on unlabeled data for which the adversary did not query the model.

We compare the accuracy of models trained with the rotation loss on data labeled by the oracle and data with ImageNet labels. Our best performing extracted model, with an accuracy of 64.5%, is trained with the rotation loss on oracle labels whereas the baseline on ImageNet labels only achieves 62.5% accuracy with the rotation loss and 61.2% without the rotation loss. This demonstrates the cumulative benefit of adding a rotation loss to the objective and training on oracle labels for a theft-motivated adversary.

We note that as semi-supervised learning techniques on ImageNet mature, further gains should be reflected in the performance of model extraction attacks.

MixMatch. To validate this hypothesis, we turn to smaller scale datasets where semi-supervised learning has already made significant progress. We investigate a technique called MixMatch [37] on two datasets: SVHN [38] and CIFAR10 [39].

For both datasets, inputs are color images of 32x32 pixels that need to be classified in 10 classes. The training set of SVHN contains 73257 images (50000 for CIFAR10) and the test set contains 26032 images (10000 for CIFAR10). We train the oracle with a WideResNet-28-2 architecture on the labeled training set. This achieves 97.36% accuracy on SVHN and 95.75% accuracy on CIFAR10.

The adversary is given access to the same training set but without knowledge of the labels. Our goal is to validate the effectiveness of semi-supervised learning by demonstrating that the adversary only needs to query the oracle on a small subset of these training points to extract a model whose accuracy on the task is comparable to the oracle’s. To this end, we run 5 trials of fully supervised extraction (no use of unlabeled data), and 5 trials of MixMatch, reporting for each trial the median accuracy of the 20 latest checkpoints, as done in [37].

Results. With only 250 queries (293x smaller label set than the SVHN oracle and 200x smaller for CIFAR10), MixMatch reaches 95.82% test accuracy on SVHN and 87.98% accuracy on CIFAR10. This is higher than fully supervised training that uses 4000 queries. With 4000 queries, MixMatch is within 0.29% of the accuracy of the oracle on SVHN, and 2.46% on CIFAR10. The variance of MixMatch is slightly higher than that of fully supervised training, but is much smaller than the

¹We can’t follow the distillation procedure from [24] exactly because we have access to the output probabilities of the oracle rather than its logits, making it impossible to directly control the softmax temperature.

²<https://paperswithcode.com/sota/image-classification-on-imagenet>

Architecture	Data Fraction	ImageNet	WSL	WSL-5	ImageNet + Rot	WSL + Rot	WSL-5 + Rot
Resnet_v2_50	10%	(81.86/82.95)	(82.71/84.18)	(82.97/84.52)	(82.27/84.14)	(82.76/84.73)	(82.84/84.59)
Resnet_v2_200	10%	(83.50/84.96)	(84.81/86.36)	(85.00/86.67)	(85.10/86.29)	(86.17/88.16)	(86.11/87.54)
Resnet_v2_50	100%	(92.45/93.93)	(93.00/94.64)	(93.12/94.87)	N/A	N/A	N/A
Resnet_v2_200	100%	(93.70/95.11)	(94.26/96.24)	(94.21/95.85)	N/A	N/A	N/A

TABLE II

EXTRACTION ATTACK (TOP-5 ACCURACY/TOP-5 FIDELITY) OF THE WSL MODEL, WHICH WAS TRAINED ON 1 BILLION IMAGES [28]. EACH ROW CORRESPONDS TO A PAIR OF ARCHITECTURE AND FRACTION OF PUBLIC IMAGENET DATA USED BY THE ADVERSARY TO TRAIN THE MODEL USING LABELS FROM THE WSL ORACLE. IMAGENET COLUMN REFERS TO USING ONLY IMAGENET LABELS—THIS IS A BASELINE. WSL REFERS TO AN ORACLE RETURNING PROBABILITIES OF THE WSL MODEL. WSL-5 REFERS TO AN ORACLE THAT ONLY RETURNS THE TOP 5 PROBABILITIES. COLUMNS WITH (+ ROT) REFER TO AN ADVERSARY WHO LEVERAGES UNLABELED TRAINING DATA WITH THE ROTATION LOSS [33, 34]. ROTATION LOSS WAS NOT RUN ON 100% OF TRAINING DATA BECAUSE ALL DATA IS LABELED. AN ADVERSARY ABLE TO QUERY WSL ALWAYS IMPROVES OVER IMAGENET LABELS, EVEN WITH ACCESS TO THE TOP 5 PROBABILITIES ONLY. ROTATION LOSS DOES NOT SIGNIFICANTLY IMPROVE THE PERFORMANCE ON RESNET_V2_50, BUT PROVIDES A (1.36/1.80) IMPROVEMENT FOR RESNET_V2_200, WHICH IS COMPARABLE TO THE PERFORMANCE BOOST GIVEN BY WSL LABELS ON 10% DATA. THERE IS STILL BENEFIT IN THE HIGH-DATA REGIME, WHERE WE OBSERVE A (0.56/1.13) IMPROVEMENT USING WSL LABELS.

Dataset	Algorithm	250 Queries	1000 Queries	4000 Queries
SVHN	FS	(79.25/79.48)	(89.47/89.87)	(94.25/94.71)
SVHN	MM	(95.82/96.38)	(96.87/97.45)	(97.07/97.61)
CIFAR10	FS	(53.35/53.61)	(73.47/73.96)	(86.51/87.37)
CIFAR10	MM	(87.98/88.79)	(90.63/91.39)	(93.29/93.99)

TABLE III

EXTRACTION ATTACK PERFORMANCE (ACCURACY/FIDELITY) OF FULLY SUPERVISED (FS) AND MIXMATCH (MM) EXTRACTION ON SVHN AND CIFAR10. THE SVHN ORACLE REACHES ACCURACY OF 97.36%, AND THE CIFAR10 ORACLE REACHES 95.75% ACCURACY. NOTE THAT THE BEST ACCURACY AND FIDELITY ACHIEVED BY MIXMATCH IS VERY CLOSE TO THE ORACLE’S PERFORMANCE FOR BOTH DATASETS, AND MIXMATCH AT 250 QUERIES BEATS FULLY SUPERVISED TRAINING AT 4000 QUERIES FOR BOTH DATASETS. RESULTS ARE AVERAGED OVER 5 DIFFERENT SPLITS FOR SELECTING THE DATA QUERIED.

performance gap. These gains come from the prior MixMatch is able to build using the unlabeled data, making it effective at exploiting few labels.

C. Fidelity of learning-based extracted models

We now turn to reconnaissance, where achieving high fidelity enables the adversary to mount attacks that rely on the extracted model making similar mistakes to the oracle. We consider here the label agreement with the oracle on test data.

Those improvements in accuracy from semi-supervised learning are mirrored in fidelity as well, even though no extra information about the oracle is gained when leveraging unlabeled data. When using oracle labels, the top-1 fidelity increases by 1.62% for ResNet_v2_50, and by 2.55% for ResNet_v2_200 when querying only 10% of the data. Using rotation loss increases this advantage to 2.07% for ResNet_v2_50 and 4.41% for ResNet_v2_200. Interestingly, these gains are larger than those observed for accuracy—we expect that improved semi-supervised learning techniques would continue to reap fidelity gains on ImageNet models. Fidelity also improves for the smaller datasets when using MixMatch—the smallest difference is 2.9% at 4000 queries on SVHN, and the largest is a gap of a full 25.18% on CIFAR10 at 250 queries. Again, the unlabeled data allows MixMatch to build a strong prior to improve fidelity with.

V. LIMITATIONS OF LEARNING-BASED EXTRACTION

Learning-based approaches have several sources of non-determinism—the random initializations of the model parameters, the order in which data is assembled to form batches for SGD, and even the non-determinism in GPU instructions [40, 41]. These sources of non-determinism impact the model parameter values obtained upon completion of training. This implies that even if the adversary had full access to the oracle’s training data, hyperparameters, etc., they would still need to be able to reconstruct all of the learner’s non-determinism in order to achieve perfect fidelity needed for the *functionally equivalent* extraction goal described in Section III.

We perform the following experiment. Initially query an oracle to obtain a labeled substitute dataset \mathcal{D} . Use this dataset for a learning-based extraction attack, producing a model $f_{\theta}^1(x)$. Then, run the learning-based attack a second time using the same substitute dataset, but different sources of non-determinism to obtain a new set of parameters $f_{\theta}^2(x)$. If there are points x such that $f_{\theta}^1(x) \neq f_{\theta}^2(x)$, then the prediction on x is dependent not on the oracle, but on the non-determinism of the learning-based attack strategy—we are unable to guarantee fidelity.

We independently control the initialization randomness and batch randomness during training on Fashion-MNIST [42] with fully supervised SGD (we use Fashion-MNIST for training speed). We repeated each run 5 times and measure agreement between the five obtained models on the test set.

Even when both training and initialization randomness are fixed (so that GPU non-determinism is the only source of randomness) fidelity peaks at 95%. With no randomness fixed, we achieve at worst 92% fidelity on the test set. (These 5% and 8% percent disagreements in fidelity should be taken in the context of the base accuracy of 90% test accuracy.) Hence, even an adversary who has the victim model’s *exact* training set will be unable to exceed 92% fidelity. We explore this phenomenon further in Figure 2. Using prototypicality metrics, as investigated in Carlini et al. [43], we notice that those points where fidelity is easiest to achieve are also the most prototypical (i.e., more representative of the class it is labeled as). This connection is explored further in Appendix C.

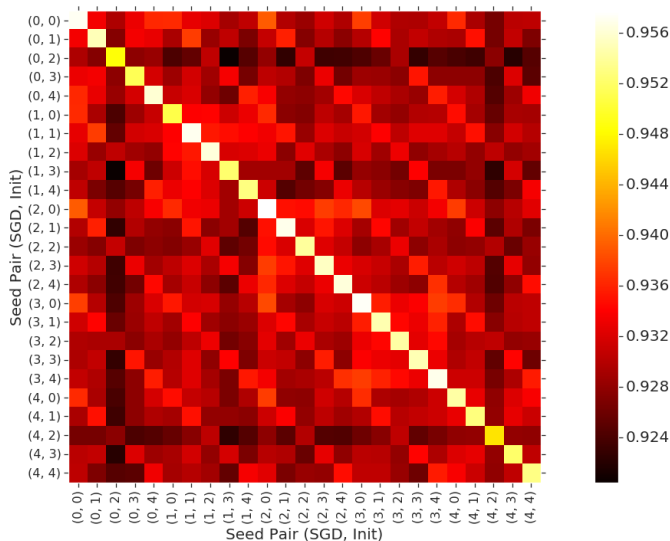


Fig. 2. Agreement between networks trained with different random initializations and training randomness. Five random weight initializations and five random seeds for SGD randomness were used, with five trials done at each pair. Pairs are arranged on the x and y axes first by SGD randomness, then by initialization randomness. Naturally, the diagonal (where all randomness is fixed) has the most agreement, but it is still only on at most 95.6% of points due to nondeterminism in various GPU instructions. The diagonals in each 5x5 block are brighter than the rest of the blocks—this indicates the importance of random initialization. Finally, some 5x5 blocks around the main diagonal are brighter than others, indicating that SGD randomness has some effect, but less so than the initialization (this is likely because GPU training already introduces a significant source of disagreement during optimization).

It follows from these arguments that non-determinism of both the victim and extracted model’s learning procedures potentially compound, limiting the effectiveness of using a learning-based approach to reaching high fidelity.

VI. FUNCTIONALLY EQUIVALENT EXTRACTION

Having identified fundamental limitations that prevent learning-based approaches from perfectly matching the oracle’s mistakes, we now turn to a different approach where the adversary extracts the oracle’s weights directly.

This attack can be seen as an extension of two prior works.

- Milli *et al.* [19] introduce an attack to extract neural network weights under the assumption that the adversary is able to make *gradient queries*. That is, each query the adversary makes reveals not only the prediction of the neural network, but also the gradient of the neural network at that query point. To the best of our knowledge this is the only functionally-equivalent extraction attack on neural networks with one hidden layer, although it was not actually implemented in practice.
- Batina *et al.* [25] introduce a side-channel attack that extracts neural network weights through monitoring the power use of a microprocessor evaluating the neural network. This is a much more powerful threat model than made by any of the other model extraction papers. To the best of our knowledge this is the only practical

Symbol	Definition
d	Input dimensionality
h	Hidden layer dimensionality ($h < d$)
K	Number of classes
$A^{(0)} \in \mathbb{R}^{d \times h}$	Input layer weights
$B^{(0)} \in \mathbb{R}^h$	Input layer bias
$A^{(1)} \in \mathbb{R}^{h \times K}$	Logit layer weights
$B^{(1)} \in \mathbb{R}^K$	Logit layer bias

TABLE IV
PARAMETERS FOR THE FUNCTIONALLY-EQUIVALENT ATTACK.

direct model extraction result—they manage to extract essentially arbitrary depth networks.

In this section we introduce an attack which only requires standard queries (i.e., that return the model’s prediction instead of its gradients) and does not require any side-channel leakages, yet still manages to achieve *higher fidelity* extraction than the side-channel extraction work for two-layer networks, assuming double-precision inference.

a) Attack Algorithm Intuition.: As in [19], our attack is tailored to work on neural networks with the ReLU activation function (the ReLU is an effective default choice of activation function [20]). This makes the neural network a piecewise linear function. Two samples are within the same linear region if all of the ReLU units have the same sign. This is illustrated in Figure 3.

By computing the difference between adjacent hyperplanes, so that exactly one ReLU unit has flipped signs, it is possible to almost completely determine the weight vector going into that ReLU unit. By repeating this attack for all ReLU units we can therefore recover the first weight matrix completely. (We say almost here, because we must do some work to recover the sign of the weight vector.) Once the first layer of the two-layer neural network has been determined, the second layer can be uniquely solved for algebraically through least squares. This attack is optimal up to a constant factor—the query complexity is discussed in Appendix E.

A. Notation and Assumptions

As in [19], we only aim to extract neural networks with one hidden layer using the ReLU activation function. We denote the model weights by $A^{(0)} \in \mathbb{R}^{d \times h}$, $A^{(1)} \in \mathbb{R}^{h \times K}$ and biases by $B^{(0)} \in \mathbb{R}^h$, $B^{(1)} \in \mathbb{R}^K$. Here, d , h , and K respectively refer to the input dimensionality, the size of the hidden layer, and the number of classes. This is found in Table VI-A.

We say that $\text{ReLU}(x)$ is at a critical point if $x = 0$; this is the location at which the units gradient changes from 0 to 1.

We assume the adversary is able to observe the raw logit outputs as 64-bit floating point values. We will use the notation \mathcal{O}_L to denote the logit oracle. Our attack implicitly assumes that the rows of $A^{(0)}$ are linearly independent. Because the dimensional of the input space is larger than the hidden space by at least 100, it is exceedingly unlikely for the rows to be linearly dependent (and we find this holds true in practice).

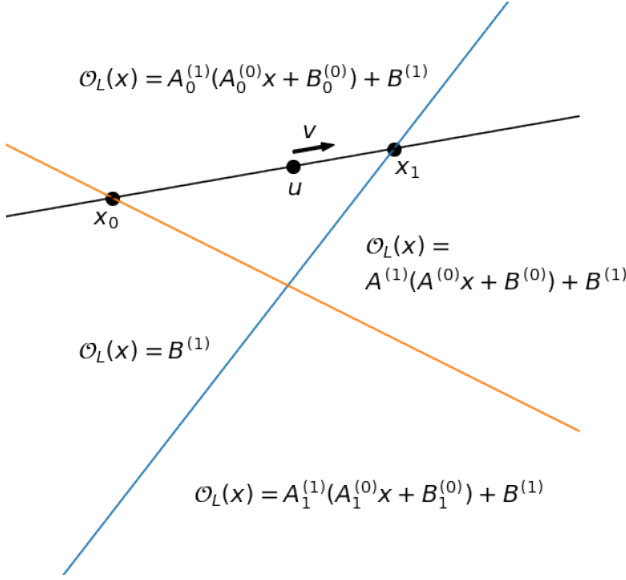


Fig. 3. 2-dimension intuition for the functionally equivalent extraction attack.

We remark that our attack is not an SQ algorithm, which would require us to only look at aggregate statistics of our dataset: instead, we require highly local analysis of the network. This algorithmic structure, and the preceding assumptions, allow us to avoid the pathologies of Section III-C1.

B. Attack Overview

The algorithm is broken into four phases:

- **Critical point search** identifies inputs $\{x_i\}_{i=1}^n$ to the neural network so that exactly one of the ReLU units is at a critical point (i.e., has input identically 0).
- **Weight recovery** takes an input x which causes the i th neuron to be at a critical point. We use this point x to compute the difference between the two adjacent hyperplanes induced by the critical point, and thus the weight vector row $A_i^{(0)}$. By repeating this process for each ReLU we obtain the complete matrix $A^{(0)}$. Due to technical reasons discussed below, we can only recover the row-vector up to sign.
- **Sign recovery** determines the sign of each row-vector $A_j^{(0)}$ for all j using global information about the complete weight matrix $A^{(0)}$.
- **Final layer extraction** uses algebraic techniques (e.g., least squares) to solve for the second layer of the network.

C. Critical Point Search

For a two layer network, observe that the logit function is given by the equation $\mathcal{O}_L(x) = A^{(1)}\text{ReLU}(A^{(0)}x + B^{(0)}) + B^{(1)}$. To find a critical point for every ReLU, we sample two random vectors $u, v \in \mathbb{R}^d$, and consider the function

$$L(t; u, v, \mathcal{O}_L) = \mathcal{O}_L(u + tv).$$

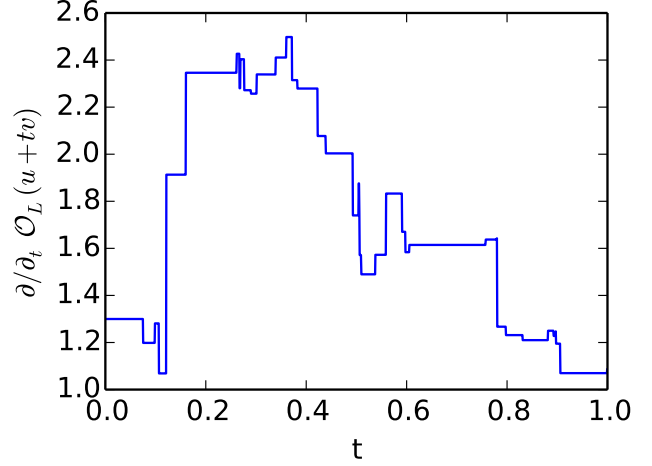


Fig. 4. An example sweep for critical point search. Here we plot the partial derivative across t and see that $\mathcal{O}_L(u + tv)$ is piecewise linear, enabling a binary search.

for t varying between a small and large appropriately selected value (discussed below). $L(\cdot)$ is a piecewise linear function, and that the points t where $L(t)$ is non-differentiable are exactly locations where some ReLU_i is changing signs (i.e., some ReLU is at a critical point). Figure 4 shows an example of what this sweep looks like on a trained MNIST model.

Furthermore, notice that given a pair u, v , there is exactly one value t for which each ReLU is at a critical point, and if t is allowed to grow arbitrarily large or small that every ReLU unit will switch sign exactly once. Intuitively, the reason this is true is that each ReLU's input is either a monotonically increasing or decreasing function of t . Thus, by varying t , we can identify an input x_i that sets the i th ReLU to 0 for every relu i in the network. This assumes we are not moving parallel to any of the rows, and that we vary t within a sufficiently large interval. The analysis of [19] suggests that these concerns can be resolved with high probability by varying $t \in [-h^2, h^2]$.

While in theory it would be possible to sweep all values of t to identify the critical points, this would require a large number of queries. Thus, to efficiently search for the locations of critical points, we introduce a refined search algorithm which improves on the binary search as used in [19]. Standard binary search requires $O(n)$ model queries to obtain n bits of precision. Therefore, we propose a refined technique which does not have this restriction and requires just $O(1)$ queries to obtain high (20+ bits) precision. The key observation we make is that if we are searching between two values $[t_1, t_2]$ and there is exactly one discontinuity in this range, we can precisely identify the location of that discontinuity efficiently. The property this leverages is that the function is piecewise linear - if we know the range is composed of two linear segments, we can compute where they intersect. An intuitive diagram for this algorithm can be found in Figure 5 and the algorithm can be found in Algorithm 1.

D. Weight Recovery

After running critical point search we obtain a set $\{x_i\}_{i=1}^h$, where each critical point corresponds to a point where a single ReLU flips sign. In order to use this information to learn the weight matrix $A^{(0)}$ we measure the second derivative of \mathcal{O}_L in each input direction at the points x_i . Taking the second derivative here corresponds to measuring the difference between the linear regions on either side of the ReLU. Recall that prior work assumed direct access to gradient queries, and thus did not require any of the analysis in this section.

1) *Absolute Value Recovery*: To formalize the intuition of comparing adjacent hyperplanes, observe that for the oracle \mathcal{O}_L and for a critical point x_i (corresponding to ReLU_i being zero) and for a random input-space direction e_j we have

$$\begin{aligned} \left. \frac{\partial^2 \mathcal{O}_L}{\partial e_j^2} \right|_{x_i} &= \left. \frac{\partial \mathcal{O}_L}{\partial e_j} \right|_{x_i + c \cdot e_j} - \left. \frac{\partial \mathcal{O}_L}{\partial e_j} \right|_{x_i - c \cdot e_j} \\ &= \sum_k A_k^{(1)} \mathbb{1}(A_k^{(0)}(x_i + c \cdot e_j) + B_k^{(0)} > 0) A_{kj}^{(0)} \\ &\quad - \sum_k A_k^{(1)} \mathbb{1}(A_k^{(0)}(x_i - c \cdot e_j) + B_k^{(0)} > 0) A_{kj}^{(0)} \\ &= A_i^{(1)} \left(\mathbb{1}(A_i^{(0)} \cdot e_j > 0) - \mathbb{1}(-A_i^{(0)} \cdot e_j > 0) \right) A_{ji}^{(0)} \\ &= \pm (A_{ji}^{(0)} A_i^{(1)}) \end{aligned}$$

for a $c > 0$ small enough so that $x_i \pm c \cdot e_j$ does not flip any other ReLU. Because x_i is a critical point and c is small, the sums in the second line differ only in the contribution of ReLU_i . We’ve only recovered a product involving both weight matrices. Let’s see how we can use this information.

If we compute $|A_{1i}^{(0)} A^{(1)}|$ and $|A_{2i}^{(0)} A^{(1)}|$ by querying along directions e_1 and e_2 , we can divide these quantities to obtain the value $|A_{1i}^{(0)} / A_{2i}^{(0)}|$, the ratio of the two weights. By repeating the above process for each input direction we can, for all k , obtain the pairwise ratios $|A_{1i}^{(0)} / A_{ki}^{(0)}|$.

Recall from Section III that obtaining the ratios of weights is the theoretically optimal result we could hope to achieve. It is always possible to multiply all of the weights *into* a ReLU by a constant $c > 0$ and then multiply all of the weights *out* of the ReLU by c^{-1} . Thus, without loss of generality, we can assign $A_{1i}^{(0)} = 1$ and scale the remaining entries accordingly. Unfortunately, we have lost a small amount of information here. We have only learned the absolute value of the ratio, and not the value itself.

2) *Weight Sign Recovery*: Once we reconstruct the values $|A_{ji}^{(0)} / A_{1i}^{(0)}|$ for all j we need to recover the sign of these values. To do this we consider the following quantity:

$$\left. \frac{\partial^2 \mathcal{O}_L}{\partial (e_j + e_k)^2} \right|_{x_i} = \pm (A_{ji}^{(0)} A_i^{(1)} \pm A_{ki}^{(0)} A_i^{(1)}).$$

That is, we consider what would happen if we take the second partial derivative in the direction $(e_j + e_k)$. Their contributions to the gradient will either cancel out, indicating $A_{ji}^{(0)}$ and $A_{ki}^{(0)}$ are of opposite sign, or they will compound on each other,

indicating they have the same sign. Thus, to recover signs, we can perform this comparison along each direction $(e_1 + e_j)$.

Here we encounter one final difficulty. There are a total of n signs we need to recover, but because we compute the signs by comparing ratios along different directions, we can only obtain $n - 1$ relations. That is, we now know the correct signed value of $A_i^{(0)}$ up to a single sign for the entire row.

It turns out this is to be expected. What we have computed is the normal direction to the hyperplane, but because any given hyperplane can be described by an infinite number of normal vectors differing by a constant scalar, we can not hope to use local information to recover this final sign bit.

Put differently, while it is possible to push a constant $c > 0$ through from the first layer to the second layer, it is not possible to do this for negative constants, because the ReLU function is not symmetric. Therefore, it is necessary to learn the sign of this row.

E. Global Sign Recovery

Once we have recovered the input vector’s weights, we still don’t know the sign for the given inputs - we only measure the difference between linear functions at each critical point, but do not know which side is the positive side of the ReLU [19]. Now, we need to leverage global information in order to reconcile all of inputs’ signs.

Notice that recovering $\hat{A}_i^{(0)}$ allows us to obtain $B_i^{(0)}$ by using the fact that $A_i^{(0)} \cdot x_i + B_i^{(0)} = 0$. Then we can compute $\hat{B}_i^{(0)}$ up to the same global sign as is applied to $\hat{A}_i^{(0)}$.

To begin we search for a vector z that is in the null space of $\hat{A}^{(0)}$, that is, $\hat{A}^{(0)} z = \vec{0}$. Because the neural network has $h < d$, the null-space is non-zero, and we can find many such vectors through least squares. Then, for each ReLU_i we search for a vector v_i such that $v_i A^{(0)} = e_i$ where here e_i is the i th basis vector in the hidden space. That is, moving along the v_i direction only changes ReLU_i ’s input value. Again we can search for this through least squares.

Given z and these v_i we query the neural network for the values of $\mathcal{O}_L(z)$, $\mathcal{O}_L(z + v_i)$, and $\mathcal{O}_L(z - v_i)$. On each of these three queries, all hidden units are 0 except for ReLU_i which receives as input either 0, 1, or -1 by the construction of v_i . However, notice that the output of ReLU_i can only be either 0 or 1, and the two $\{-1, 0\}$ cases collapse to just output 0. Therefore, if $\mathcal{O}_L(z + v_i) = \mathcal{O}_L(z)$, we know that $A_i^{(0)} \cdot v_i < 0$. Otherwise, we know $\mathcal{O}_L(z - v_i) = \mathcal{O}_L(z)$ and $A_i^{(0)} \cdot v_i > 0$. This allows us to recover the sign bit for ReLU_i .

F. Last Layer Extraction

Once we have fully specified the function to compute the first hidden layer, the logit function of the network is just a linear transformation which we can recover with least squares, through making h queries where each ReLU is active at least once. In practice, we use the critical points discovered in the previous section so that we do not need to make additional neural network queries.

Algorithm 1 Algorithm for 2-linearity testing. Computes the location of the only critical point in a given range or rejects if there is more than one.

```

Function  $f$ , range  $[t_1, t_2]$ ,  $\epsilon$ 
 $m_1 = \frac{f(t_1+\epsilon)-f(t_1)}{\epsilon}$  ▷ Gradient at  $t_1$ 
 $m_2 = \frac{f(t_2)-f(t_2-\epsilon)}{\epsilon}$  ▷ Gradient at  $t_2$ 
 $y_1 = f(a), y_2 = f(b)$ 
 $x = a + \frac{y_2-y_1-(b-a)m_2}{m_1-m_2}$  ▷ Candidate critical point
 $\hat{y} = y_1 + m_1 \frac{y_2-y_1-(b-a)m_2}{m_1-m_2}$  ▷ Function value at candidate
 $y = f(x)$  ▷ True value at candidate
if  $\hat{y} = y$  then return  $x$ 
else return "More than one critical point"
end if

```

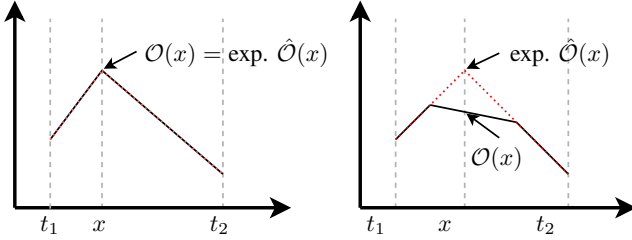


Fig. 5. Efficient and accurate 2-linearity testing subroutine in Algorithm 1. Left shows a successful case where the algorithm succeeds; right shows a potential failure case, where there are multiple nonlinearities. We detect this by observing the expected value of $O(x)$ is not the observed (queried) value.

G. Results

Setup. We train several one-layer fully-connected neural networks with between 16 and 512 hidden units (for twelve thousand and a hundred thousand trainable parameters, respectively) on the MNIST [44] and CIFAR-10 datasets [39]. We train the models with the Adam [23] optimizer for 20 epochs at batch size 128 until they converge. We train five networks of each size to obtain higher statistical significance.

MNIST		CIFAR-10	
Hidden Size	Accuracy	Hidden Size	Accuracy
16	94.3%	16	29.2%
32	95.6%	32	34.2%
64	97.2%	64	40.3%
128	97.7%	128	42.6%
512	98.3%	512	45.9%

TABLE V
STATISTICS FOR THE ORACLE MODELS WE TRAIN TO EXTRACT.

MNIST Extraction. We implement the functionally-equivalent extraction attack in JAX [45] and run it on each trained oracle. We evaluate the fidelity of the extracted model (by comparing the predictions to the oracle’s predictions) on both the standard MNIST test dataset \mathcal{X} as well as perturbed test sets

$$\mathcal{X}_\sigma = \{x + \mathcal{N}(0, I\sigma^2) : x \in \mathcal{X}\}$$

where I is the 784×784 identity matrix. That is, \mathcal{X}_σ adds Gaussian noise component-wise (to each pixel) of each image in the test set.

Results are summarized in Table VI. For the small network sizes, we achieve perfect fidelity, even on samples that have been perturbed by a large amount of noise. (We normalize all inputs $x \in [0, 1]^{784}$, so adding Gaussian noise with standard deviation 1.0 is enormous: the noise is now larger than the signal.) As the network size increases, the low-probability errors we encounter begin to increase in frequency. The extracted neural network still (almost) perfectly matches the original neural network on normal test data, but on randomly modified test examples it begins to disagree. We manage to reconstruct the first weight matrix to an average precision of 23 bits - we provide more results in Appendix D.

CIFAR-10 Extraction. The results for the CIFAR-10 model are nearly identical to the MNIST model. We achieve 100% test set agreement on models sized 16-64 and greater than 99% test set agreement on the models of size 128 and 512.

Comparison to Prior Work. To the best of our knowledge, this is by orders of magnitude the highest fidelity extraction of neural network weights.

The only fully-implemented neural network extraction attack we are aware of is the work of Batina *et al.* [25] who uses an electromagnetic side channels and differential power analysis to recover an MNIST neural network with neural network weights with an average error of 0.0025. In comparison, we are able to achieve an average error in the first weight matrix for a similarly sized neural network of just 0.0000009—over two thousand times more precise. To the best of our knowledge no functionally-equivalent CIFAR-10 models have been extracted in the past.

We are unable to make a comparison between the fidelity of our extraction attack and the fidelity of the attack presented in Batina *et al.* because they do not report on this number: they only report the accuracy of the extracted model and show it is similar to the original model. (We believe this strengthens our observation that comparing across accuracy and fidelity is not currently widely accepted as best practice.)

Investigating Errors. We observe that as the number of parameters that must be extracted increases, the fidelity of the model decreases. We investigate why this happens and discovered that a small fraction of the time (roughly 1 in 10,000) the gradient estimation procedure obtains an incorrect estimate of the gradient and therefore one of the extracted weights $\hat{A}_{ij}^{(0)}$ is incorrect by a non-insignificant margin.

Introducing an error into just one of the weights of the first matrix should not induce significant further errors. However, because of this error, when we solve for the bias vector, the extracted bias $\hat{B}_i^{(0)}$ will have error proportional to the error of $\hat{A}_{ij}^{(0)}$. And when the bias is wrong, it impacts *every* calculation.

Resolving this issue completely either requires reducing the failure rate of gradient estimation from 1 in 10,000 to practically 0, or would require a complex error-recovery procedure. Instead, we will introduce in the following section an improvement which almost completely solves this issue.

Number of Parameters	Fidelity on Test Data	Fidelity on Test Data plus $\mathcal{N}(0, I\sigma^2)$			
		$\sigma = .1$	$\sigma = .25$	$\sigma = .5$	$\sigma = 1.0$
16	100%	100%	100%	100%	100%
32	100%	100%	100%	100%	99.78%
64	100%	100%	99.96%	99.47%	92.69%
128	99.98%	99.98%	99.97%	97.51%	80.69%

TABLE VI

FIDELITY OF THE FUNCTIONALLY-EQUIVALENT EXTRACTION ATTACK ACROSS DIFFERENT TEST DISTRIBUTIONS ON AN MNIST VICTIM MODEL. RESULTS ARE AVERAGED OVER FIVE EXTRACTION ATTACKS. FOR SMALL MODELS, WE ACHIEVE PERFECT FIDELITY EXTRACTION; LARGER MODELS HAVE NEAR-PERFECT FIDELITY ON THE TEST DATA DISTRIBUTION, BUT ON NOISY DISTRIBUTIONS HAVE LOWER FIDELITY. COMPARE TO TABLE VII FOR AN IMPROVED VERSION OF THIS ATTACK WHICH ALSO ACHIEVES NEAR-PERFECT FIDELITY ON LARGE NETWORKS.

VII. HYBRID STRATEGIES

Until now the strategies we have developed for extraction have been pure and focused entirely on learning or entirely on direct extraction. We now show that there is a continuous spectrum from which we can draw attack strategies, and these *hybrid* strategies can leverage both the query efficiency of learning extraction, and the fidelity of direct extraction.

A. Learning-Based Extraction with Gradient Matching

Milli *et al.* demonstrate that *gradient matching* is an effective way to leverage model explanations. Their approach optimizes the following objective:

$$\sum_{i=1}^n H(\mathcal{O}(x_i), f(x_i)) + \alpha \|\nabla_x \mathcal{O}(x_i) - \nabla_x f(x_i)\|_2^2,$$

assuming the adversary can query the model for $\nabla_x \mathcal{O}(x)$. This is more model access than we permit our adversary, but is an example of using intuition from direct recovery to improve extraction. We found in preliminary experiments that this technique can improve fidelity on small datasets (increasing fidelity from 95% to 96.5% on Fashion-MNIST), but we leave scaling and removing the model access assumption of this technique to future work. This is not the only way that learning and direct recovery can be combined. We show next how learning can help alleviate some of the limitations of the previous functionally-equivalent extraction attack.

B. Functionally-Equivalent Error Recovery through Learning

Recall from earlier that the functionally-equivalent extraction attack fidelity degrades as the model size increases. This is a result of low-probability errors in the first weight matrix inducing incorrect biases on the first layer, which in turn propagates and causes worse errors in the second layer.

We now introduce a method for performing a learning-based error recovery routine. While performing a fully-learning-based attack leaves too many free variables so that functionally-equivalent extraction is not possible, if we fix many of the variables to the values extracted through the direct recovery attack, we now show it is possible to learn the remainder of the variables.

Number of Parameters	Fidelity on Test Data	Fidelity on Test Data plus $\mathcal{N}(0, I\sigma^2)$			
		$\sigma = .1$	$\sigma = .25$	$\sigma = .5$	$\sigma = 1.0$
16	100%	100%	100%	100%	100%
32	100%	100%	100%	99.99%	99.85%
64	100%	100%	100%	99.99%	99.79%
128	100%	100%	100%	99.94%	99.76%
512	99.31%	99.22%	98.01%	93.08%	86.37%

TABLE VII

FIDELITY OF EXTRACTED MNIST MODEL WITH HYBRID STRATEGY, COMPARE TO TABLE VI. ERROR RATES ARE REDUCED BY ORDERS OF MAGNITUDE ON HIGHLY OUT-OF-DISTRIBUTION DATA. NOTE THE LAST ROW IS NOT PRESENT IN THE PRIOR TABLE.

Formally, let $\hat{A}^{(0)}$ be the extracted weight matrix for the first layer and $\hat{B}^{(0)}$ be the extracted bias vector for the first layer. Previously, we used least squares to directly solve for $\hat{A}^{(1)}$ and $\hat{B}^{(1)}$ assuming we had extracted the first layer perfectly. Here, we relax this assumption. Instead, we perform gradient descent optimizing for parameters $W_{0..2}$ that minimize

$$\mathbb{E}_{x \in \mathcal{D}} \|f_{\theta}(x) - W_1 \text{ReLU}(\hat{A}^{(0)}x + \hat{B}^{(0)} + W_0) + W_2\|$$

That is, we use a single trainable parameter to adjust the bias term of the first layer, and then solve (via gradient descent with training data) for the remaining weight matrix accordingly.

This hybrid strategy increases the fidelity of the extracted model substantially, detailed in Table VII. In the worst-performing example from earlier (with only direct extraction) the extracted 128-neuron network had 80% fidelity agreement with the victim model. When performing learning-based recovery, the fidelity agreement jumps all the way to 99.75%.

VIII. DEFENDING AGAINST MODEL EXTRACTION

There is a fundamental tension between providing useful queries and preventing model extraction. Preventing model extraction requires decreasing the quality of the queries, but decreasing the quality of the queries too much impacts the benign user, reducing their incentive to use the model. Then there are two potential avenues for protecting against model extraction—limiting the information the adversary learns, and differentiating a benign user from a model extraction attack.

A. Information per Dollar

While completely preventing model extraction is infeasible, it may be possible to increase the cost of model extraction to a level comparable to the cost of data labeling, while balancing this with potential harm to legitimate users. The first approach to protection is to limit the amount of information an adversary learns about the model with some fixed cost. Several existing proposals in the literature use this approach. Perturbing (or rounding/adding noise to) class probabilities [11, 13, 46], releasing probabilities only for high probability classes [11], and releasing only class outputs [11, 13] have all been proposed as countermeasures. One can also sample from a distribution over model parameters [13, 47]. These approaches have not been shown to defeat model extraction, but they may force an adversary to make more queries.

In our work, the strategies presented in Sections IV and VI both assume that the adversary is able to observe the full prediction vector. Extending the functionally equivalent attack of Section VI to work with more limited information would be nontrivial—we leave this to future work. However, in Table II, we report the resilience of our learning-based extraction attack on ImageNet to only receiving probabilities for the top-5 classes. With 10% of the training data, we find only receiving top-5 labels does not significantly impact the attack’s performance—ResNet_v2_50 actually improves by 0.31% over the full prediction vector, and ResNet_v2_200 improves by 0.19%, although the improvement from rotation loss does decrease by 0.25%. The results are only slightly changed by removing access, and sometimes improve, which could be the result of the model being more “focused” on the top-5 predictions. We discuss the top-1 performance in Appendix B, where performance drops 1.19% in one case. All results are similar for fidelity.

If an adversary is forced to make more queries, it is possible for the model owner to simultaneously increase the cost of a query to thwart the adversary’s economic incentives. Prior work [13] has investigated the monetary cost of running their extraction attacks—this could lead to interesting analysis relating to adversarial objectives. For a theft-motivated adversary, the economic point of comparison would be with a human labeler. For example, the Google Cloud Vision API charges \$1.50 per 1000 model queries; Google Cloud also offers dataset labeling services at \$35 per 1000 labels—a theft-motivated adversary’s incentives point clearly to model extraction. For a reconnaissance-motivated adversary, the cost of the attack must be weighed with the economic benefit—for an adversary attempting to evade a spam classifier, their economic benefit is the expected value of the spam.

B. Differentiating Users

Another approach would be to differentiate a benign user from a malicious user who is attempting model extraction. If this is possible, it puts the model owner in a better economic position—they can offer better per-query prices if they know the user is not attempting an extraction attack. Two possible approaches are to analyze query patterns [48, 49] or use an independent authentication channel.

Looking only at query patterns is a limited approach. Given only query patterns, a nonadaptive model extraction attack (for example, equation solving or nonadaptive MixMatch training) cannot be distinguished from a benign user; however, this forces the adversary to be nonadaptive, which increases their query requirement. Even an adaptive attack (such as the attack from Section VI or an active learning based approach) could be distributed among users in a Sybil attack—this would be hard to detect, but would require the investment of account generation for the Sybils.

The other possibility is some independent authentication channel—for example, a contract between the model owner and the user. We mention this only for completeness, as this is a highly domain-dependent solution.

IX. RELATED WORK

We presented existing approaches to model extraction in Table I, and defenses in Section VIII.

Most prior work into model extraction has used learning-based techniques. This includes nonadaptive techniques [11, 12, 16] as well as adaptive techniques using various forms of active learning [7, 11–13, 15, 50]. Work that has opted for direct recovery instead has been developed for decision trees [11], linear models [8, 11], and has been theoretically proposed for two-layer neural networks [19]. Alternative threat models have been proposed for model extraction using model explanations [19] or side channel attacks [25], both of which our work builds off of.

It is also possible to query a model to steal hyperparameters [51] or architectural information [14]. An adversary that can use side channel attacks can do the same [18, 25]. These are orthogonal to our work, but compatible with it—information about a model, such as assumptions we made in Section VI, empowers an adversary to perform extraction.

Our work is also related to the field of knowledge transfer, which builds small models with comparable performance to cumbersome models (e.g., large ensembles). This includes techniques such as distillation [24] and model compression [52]. Zero shot knowledge transfer [29] has been proposed to transfer knowledge without assumptions on training data.

Watermarking neural networks has been proposed [53, 54] to identify model extraction after-the-fact. Model extraction calls into question the utility of cryptographic protocols used to protect model weights. One such approach (which has not been realized) is obfuscation [55], where an equivalent program could be released and queried as many times as desired. A more realizable approach is secure multiparty computation, where the model owner and querying party run a protocol for each query to the model [56].

X. CONCLUSION

In this paper we characterized and explored the space of model extraction attacks on neural networks.

Our learning-based methods can effectively attack a model with several millions of parameters trained on a billion images, and allows the attacker to reduce the error rate of their model by 10%. This attack does not match perfect fidelity with the victim model due to what we show are inherent limitations of learning-based approaches: even when controlling for all software-controllable randomness, randomness on the GPU itself prohibits training identical models. In contrast, our direct functionally-equivalent extraction returns a neural network agreeing with the victim model on 100% of the test samples.

We then propose a hybrid method which unifies these two attacks, using learning-based approaches to recover from numerical instability errors when performing the functionally-equivalent extraction attack.

We believe that our work highlights many remaining open problems in model stealing, such as easing some of the adversarial capabilities required by our attacks and scaling functionally-equivalent extraction.

ACKNOWLEDGEMENTS

We would like to thank Ilya Mironov and Úlfar Erlingsson for helpful discussions over the course of this work, and Florian Tramèr for his comments on an early draft of this paper.

REFERENCES

- [1] E. Strubell, A. Ganesh, and A. McCallum, “Energy and policy considerations for deep learning in nlp,” *arXiv preprint arXiv:1906.02243*, 2019.
- [2] NVIDIA, “Megatron-lm,” <https://github.com/NVIDIA/Megatron-LM>, 2019.
- [3] A. Halevy, P. Norvig, and F. Pereira, “The unreasonable effectiveness of data,” 2009.
- [4] J. Deng, W. Dong, R. Socher, L.-J. Li, K. Li, and L. Fei-Fei, “Imagenet: A large-scale hierarchical image database,” in *2009 IEEE conference on computer vision and pattern recognition*. Ieee, 2009, pp. 248–255.
- [5] I. Sutskever, O. Vinyals, and Q. V. Le, “Sequence to sequence learning with neural networks,” in *Advances in neural information processing systems*, 2014, pp. 3104–3112.
- [6] A. Van Den Oord, S. Dieleman, H. Zen, K. Simonyan, O. Vinyals, A. Graves, N. Kalchbrenner, A. W. Senior, and K. Kavukcuoglu, “Wavenet: A generative model for raw audio,” *SSW*, vol. 125, 2016.
- [7] N. Papernot, P. McDaniel, I. Goodfellow, S. Jha, Z. B. Celik, and A. Swami, “Practical black-box attacks against machine learning,” in *Proceedings of the 2017 ACM on Asia conference on computer and communications security*. ACM, 2017, pp. 506–519.
- [8] D. Lowd and C. Meek, “Adversarial learning,” in *Proceedings of the eleventh ACM SIGKDD international conference on Knowledge discovery in data mining*. ACM, 2005, pp. 641–647.
- [9] R. Shokri, M. Stronati, C. Song, and V. Shmatikov, “Membership inference attacks against machine learning models,” in *2017 IEEE Symposium on Security and Privacy (SP)*. IEEE, 2017, pp. 3–18.
- [10] A. Salem, Y. Zhang, M. Humbert, P. Berrang, M. Fritz, and M. Backes, “MI-leaks: Model and data independent membership inference attacks and defenses on machine learning models,” *arXiv preprint arXiv:1806.01246*, 2018.
- [11] F. Tramèr, F. Zhang, A. Juels, M. K. Reiter, and T. Ristenpart, “Stealing machine learning models via prediction apis,” in *25th {USENIX} Security Symposium ({USENIX} Security 16)*, 2016, pp. 601–618.
- [12] T. Orekondy, B. Schiele, and M. Fritz, “Knockoff nets: Stealing functionality of black-box models,” in *Proceedings of the IEEE Conference on Computer Vision and Pattern Recognition*, 2019, pp. 4954–4963.
- [13] V. Chandrasekaran, K. Chaudhuri, I. Giacomelli, S. Jha, and S. Yan, “Model extraction and active learning,” *CoRR*, vol. abs/1811.02054, 2018. [Online]. Available: <http://arxiv.org/abs/1811.02054>
- [14] S. J. Oh, M. Augustin, B. Schiele, and M. Fritz, “Towards reverse-engineering black-box neural networks,” *arXiv preprint arXiv:1711.01768*, 2017.
- [15] S. Pal, Y. Gupta, A. Shukla, A. Kanade, S. K. Shevade, and V. Ganapathy, “A framework for the extraction of deep neural networks by leveraging public data,” *CoRR*, vol. abs/1905.09165, 2019. [Online]. Available: <http://arxiv.org/abs/1905.09165>
- [16] J. R. Correia-Silva, R. F. Berriel, C. Badue, A. F. de Souza, and T. Oliveira-Santos, “Copycat cnn: Stealing knowledge by persuading confession with random non-labeled data,” in *2018 International Joint Conference on Neural Networks (IJCNN)*. IEEE, 2018, pp. 1–8.
- [17] C. Song and V. Shmatikov, “Overlearning reveals sensitive attributes,” *arXiv preprint arXiv:1905.11742*, 2019.
- [18] S. Hong, M. Davinroy, Y. Kaya, S. N. Locke, I. Rackow, K. Kulda, D. Dachman-Soled, and T. Dumitras, “Security analysis of deep neural networks operating in the presence of cache side-channel attacks,” *arXiv preprint arXiv:1810.03487*, 2018.
- [19] S. Milli, L. Schmidt, A. D. Dragan, and M. Hardt, “Model reconstruction from model explanations,” *arXiv preprint arXiv:1807.05185*, 2018.
- [20] V. Nair and G. E. Hinton, “Rectified linear units improve restricted boltzmann machines,” in *Proceedings of the 27th international conference on machine learning (ICML-10)*, 2010, pp. 807–814.
- [21] Y. E. Nesterov, “A method for solving the convex programming problem with convergence rate $O(1/k^2)$,” in *Dokl. akad. nauk Sssr*, vol. 269, 1983, pp. 543–547.
- [22] J. Duchi, E. Hazan, and Y. Singer, “Adaptive subgradient methods for online learning and stochastic optimization,” *Journal of Machine Learning Research*, vol. 12, no. Jul, pp. 2121–2159, 2011.
- [23] D. P. Kingma and J. Ba, “Adam: A method for stochastic optimization,” *arXiv preprint arXiv:1412.6980*, 2014.
- [24] G. Hinton, O. Vinyals, and J. Dean, “Distilling the knowledge in a neural network,” *arXiv preprint arXiv:1503.02531*, 2015.
- [25] L. Batina, S. Bhasin, D. Jap, and S. Picek, “Csi neural network: Using side-channels to recover your artificial neural network information,” *arXiv preprint arXiv:1810.09076*, 2018.
- [26] P. Kocher, J. Jaffe, and B. Jun, “Differential power analysis,” in *Annual International Cryptology Conference*. Springer, 1999, pp. 388–397.
- [27] A. Das, S. Gollapudi, R. Kumar, and R. Panigrahy, “On the learnability of deep random networks,” *CoRR*, vol. abs/1904.03866, 2019. [Online]. Available: <http://arxiv.org/abs/1904.03866>
- [28] D. Mahajan, R. Girshick, V. Ramanathan, K. He, M. Paluri, Y. Li, A. Bharambe, and L. van der Maaten, “Exploring the limits of weakly supervised pretraining,” in *Proceedings of the European Conference on Computer Vision (ECCV)*, 2018, pp. 181–196.
- [29] P. Micaelli and A. Storkey, “Zero-shot knowledge transfer via adversarial belief matching,” *arXiv preprint arXiv:1905.09768*, 2019.
- [30] A. Radford, J. Wu, R. Child, D. Luan, D. Amodei, and I. Sutskever, “Language models are unsupervised multitask learners,” *OpenAI Blog*, vol. 1, no. 8, 2019.
- [31] A. Sharif Razavian, H. Azizpour, J. Sullivan, and S. Carlsson, “Cnn features off-the-shelf: an astounding baseline for recognition,” in *Proceedings of the IEEE conference on computer vision and pattern recognition workshops*, 2014, pp. 806–813.
- [32] J. Devlin, M.-W. Chang, K. Lee, and K. Toutanova, “Bert: Pre-training of deep bidirectional transformers for language understanding,” *arXiv preprint arXiv:1810.04805*, 2018.
- [33] S. Gidaris, P. Singh, and N. Komodakis, “Unsupervised representation learning by predicting image rotations,” *arXiv preprint arXiv:1803.07728*, 2018.
- [34] X. Zhai, A. Oliver, A. Kolesnikov, and L. Beyer, “S4l: Self-supervised semi-supervised learning,” *arXiv preprint arXiv:1905.03670*, 2019.
- [35] D. Angluin, “Queries and concept learning,” *Machine learning*, vol. 2, no. 4, pp. 319–342, 1988.
- [36] A. Blum and T. Mitchell, “Combining labeled and unlabeled data with co-training,” in *Proceedings of the eleventh annual conference on Computational learning theory*. Citeseer, 1998, pp. 92–100.
- [37] D. Berthelot, N. Carlini, I. Goodfellow, N. Papernot, A. Oliver, and C. Raffel, “Mixmatch: A holistic approach to semi-supervised learning,” *arXiv preprint arXiv:1905.02249*, 2019.
- [38] Y. Netzer, T. Wang, A. Coates, A. Bissacco, B. Wu, and A. Y. Ng, “Reading digits in natural images with unsupervised feature learning,” 2011.
- [39] A. Krizhevsky *et al.*, “Learning multiple layers of features from tiny images,” Citeseer, Tech. Rep., 2009.
- [40] D. Sculley, G. Holt, D. Golovin, E. Davydov, T. Phillips, D. Ebner, V. Chaudhary, M. Young, J.-F. Crespo, and D. Dennison, “Hidden technical debt in machine learning systems,” in *Advances in neural information processing systems*, 2015, pp. 2503–2511.
- [41] B. Lakshminarayanan, A. Pritzel, and C. Blundell, “Simple and scalable predictive uncertainty estimation using deep ensembles,” in *Advances in Neural Information Processing Systems*, 2017, pp. 6402–6413.
- [42] H. Xiao, K. Rasul, and R. Vollgraf, (2017) Fashion-mnist: a novel image dataset for benchmarking machine learning algorithms.
- [43] N. Carlini, U. Erlingsson, and N. Papernot, “Prototypical examples in deep learning: Metrics, characteristics, and utility,” 2019. [Online]. Available: <https://openreview.net/forum?id=1xyx3R9tQ>
- [44] Y. LeCun, L. Bottou, Y. Bengio, P. Haffner *et al.*, “Gradient-based learning applied to document recognition,” *Proceedings of the IEEE*, vol. 86, no. 11, pp. 2278–2324, 1998.
- [45] Google, “Jax,” <https://github.com/google/jax>, 2019.
- [46] T. Lee, B. Edwards, I. Molloy, and D. Su, “Defending against model stealing attacks using deceptive perturbations,” *arXiv preprint arXiv:1806.00054*, 2018.
- [47] I. M. Alabdulmohsin, X. Gao, and X. Zhang, “Adding robustness to support vector machines against adversarial reverse engineering,” in *Proceedings of the 23rd ACM International Conference on Conference on Information and Knowledge Management*. ACM, 2014, pp. 231–240.

- [48] M. Juuti, S. Szyller, A. Dmitrenko, S. Marchal, and N. Asokan, "Prada: protecting against dnn model stealing attacks," *arXiv preprint arXiv:1805.02628*, 2018.
- [49] M. Kesarwani, B. Mukhoty, V. Arya, and S. Mehta, "Model extraction warning in mlaas paradigm," in *Proceedings of the 34th Annual Computer Security Applications Conference*. ACM, 2018, pp. 371–380.
- [50] T. S. Sethi and M. Kantardzic, "Data driven exploratory attacks on black box classifiers in adversarial domains," *Neurocomputing*, vol. 289, pp. 129–143, 2018.
- [51] B. Wang and N. Z. Gong, "Stealing hyperparameters in machine learning," in *2018 IEEE Symposium on Security and Privacy (SP)*. IEEE, 2018, pp. 36–52.
- [52] C. Bucilua, R. Caruana, and A. Niculescu-Mizil, "Model compression," in *Proceedings of the 12th ACM SIGKDD international conference on Knowledge discovery and data mining*. ACM, 2006, pp. 535–541.
- [53] J. Zhang, Z. Gu, J. Jang, H. Wu, M. P. Stoecklin, H. Huang, and I. Molloy, "Protecting intellectual property of deep neural networks with watermarking," in *Proceedings of the 2018 on Asia Conference on Computer and Communications Security*. ACM, 2018, pp. 159–172.
- [54] Y. Uchida, Y. Nagai, S. Sakazawa, and S. Satoh, "Embedding watermarks into deep neural networks," in *Proceedings of the 2017 ACM on International Conference on Multimedia Retrieval*. ACM, 2017, pp. 269–277.
- [55] B. Barak, O. Goldreich, R. Impagliazzo, S. Rudich, A. Sahai, S. Vadhan, and K. Yang, "On the (im) possibility of obfuscating programs," in *Annual international cryptology conference*. Springer, 2001, pp. 1–18.
- [56] M. Barni, C. Orlandi, and A. Piva, "A privacy-preserving protocol for neural-network-based computation," in *Proceedings of the 8th workshop on Multimedia and security*. ACM, 2006, pp. 146–151.
- [57] G. Katz, C. Barrett, D. L. Dill, K. Julian, and M. J. Kochenderfer, "Reluplex: An efficient smt solver for verifying deep neural networks," in *International Conference on Computer Aided Verification*. Springer, 2017, pp. 97–117.

APPENDIX A FORMAL STATEMENTS FOR SECTION III-C

Here, we give the formal arguments for the difficulty of model extraction to support the informal statements made in Section III-C.

Theorem 1. *There exists a class of width $3k$ and depth 2 neural networks on domain $[0, 1]^d$ with $d \geq k$ that require 256^k queries to extract.*

In order to prove Theorem 1, we introduce a family of functions we call *k-rectangle bounded functions*, which we will show satisfies this property.

Definition A.1. *A function f on domain $[0, 1]^d$ with range \mathbb{R} is called a rectangle bounded function if there exists two vectors a, b such that $f(x) \neq 0 \implies a \preceq x \preceq b$. We use \preceq to denote element-wise comparison. The function f is called a *k-rectangle bounded function* if there are k indices i such that $a_i \neq 0$ or $b_i \neq 1$.*

Intuitively, a *k-rectangle function* only outputs a non-zero value on a multidimensional rectangle that is constrained in only k coordinates. We begin by showing that we can implement *k-rectangle functions* for any a, b using a ReLU network of width k and depth 2.

Lemma 1. *For any a, b with k indices i such that $a_i \neq 0$ or $b_i \neq 1$, we can construct a *k-rectangle bounded function* for a, b with a ReLU network of width $3k$ and depth 2.*

Proof. We will start by constructing a 3-ReLU gadget with output ≥ 1 only when $a_i \leq x_i \leq b_i$. We will then show how to compose k of these gadgets, one for each index of the *k-rectangle*, in order to construct the *k-rectangle bounded function*.

The 3-ReLU gadget only depends on x_i , so weights for all other ReLUs will be set to 0. Observe that the function $T_i(x; a, b) = \text{ReLU}(x - a) + \text{ReLU}(x_i - b_i) - 2\text{ReLU}(x_i - (a_i + b_i)/2)$ is nonzero only on the interval (a_i, b_i) . This is easier to see when it is written as

$$\begin{aligned} & \text{ReLU}(x_i - a_i) - \text{ReLU}(x_i - (a_i + b_i)/2) \\ & - (\text{ReLU}(x_i - (a_i + b_i)/2) - \text{ReLU}(x_i - b_i)). \end{aligned}$$

The function $\text{ReLU}(x - x_1) - \text{ReLU}(x - x_2)$ with $x_1 < x_2$ looks like a sigmoid, and has the following form:

$$\text{ReLU}(x - x_1) - \text{ReLU}(x - x_2) = \begin{cases} 0 & x \leq x_1 \\ x - x_1 & x_1 \leq x \leq x_2 \\ x_2 - x_1 & x \geq x_2 \end{cases}$$

Now, $T_i(x; a_i, b_i) \cdot 1/(b_i - a_i)$ has range $[0, 1]$ for any value of a_i, b_i . Then the function

$$f_{a,b}(x) = \text{ReLU}\left(\sum_i (T_i(x; a_i, b_i)/(b_i - a_i)) - (k - 1)\right)$$

is *k-rectangle bounded* for vectors a, b . To see why, we need that no input x not satisfying $a \preceq x \preceq b$ has $\sum_i (T_i(x; a_i, b_i)/(b_i - a_i)) > k - 1$. This is simply because

each term $T_i(x; a_i, b_i) \leq 1$, so unless all k such terms are > 0 , the inequality cannot hold. \square

Now that we know how to construct a k -rectangle bounded function, we will introduce a set of 256^k disjoint k -rectangle bounded functions, and then show that any one requires 256^k queries to extract when the others are in the set of possible functions.

Lemma 2. *There exists a family of k -rectangle bounded functions \mathcal{F} such that extracting an element of \mathcal{F} requires 256^k queries to extract in the worst case.*

This theorem holds for any value of 256 - we chose this number to reflect the standard setting of image classification with 8-bit pixel values.

Proof. We begin by constructing \mathcal{F} . The following 256 ranges are clearly pairwise disjoint: $\{(\frac{i-1}{256}, \frac{i}{256})\}_{i=1}^{256}$. Then pick k indices arbitrarily, and we can construct 256^k distinct k -rectangle bounded functions - one for each element in the Cartesian product of each index's set of ranges. Call this set \mathcal{F} .

The set of inputs with non-zero output is distinct for each function, because their rectangles are distinct. Now consider the information gained from any query. If the query returns a non-zero value, the function is learned. If not, at most one function from \mathcal{F} is ruled out - the function whose rectangle was queried. Then any sequence of n queries to an oracle can rule out at most n of the functions of \mathcal{F} , so that at least $|\mathcal{F}| = 256^k$ queries are required in the worst case. \square

Putting these two statements together gives us Theorem 1. Note that many other constructions are possible for an \mathcal{F} with the same qualitative statement - for example, constructing disjoint simplices in k dimensions requires a width of only $k + 1$.

Theorem 2. *Checking whether two networks with domains $\{0, 1\}^d$ are functionally equivalent is NP-hard.*

Proof. We prove this by reduction to subset sum. A similar reduction (reducing to 3-SAT instead of Subset Sum) for a different statement appears in [57].

Suppose we receive a Subset Sum instance $T, p, [v_1, v_2, \dots, v_d]$ - the set is v , the target sum is T , and the precision of the problem is p . We will construct networks f_1 and f_2 such that checking if f_1 and f_2 are functionally equivalent is equivalent to finding a solution to subset sum or returning false. We can start by setting $f_1 = 0$ - it never returns a non-zero value. We will now construct a network f_2 that will have nonzero output only if the subset sum instance can be solved (and finding an input with nonzero output reveals the satisfying subset).

The network f_2 will have three hidden units in the first layer with incoming weight for the i th feature equal to v_i . This means the dot product of the input x with weights will be the sum of the subset $\{i | x_i = 1\}$. We want to force this to

accept iff there is an input where this sum is T . To do so, we use the same 3-ReLU gadget as in the proof of Theorem 1:

$$f_2(x; T, p, v) = \text{ReLU}(x \cdot v - (T - p/2)) \\ + \text{ReLU}(x \cdot v - (T + p/2)) - 2\text{ReLU}(x \cdot v - T).$$

As before, this will only be nonzero in the range $[T - p/2, T + p/2]$, and we are done. \square

APPENDIX B EXTENDED RESULTS FOR SECTION IV

Here, we present the extended results for ImageNet, containing top-1 accuracy and fidelity for our attacks.

First, observe that using WSL labels improves both the top-1 accuracy and fidelity. For ResNet_v2_50 with 10% of the data, we see a gain of 1.02% for accuracy and 1.68% for fidelity over using ImageNet labels. For ResNet_v2_200 with 10% of the data, the improvement is larger—1.88% for accuracy and 2.59% for fidelity.

Rotation loss is also effective for top-1 metrics. For ResNet_v2_50 with 10% of the data, accuracy improves by 0.26% and fidelity by 0.39% over only using WSL labels and no unlabeled data. For ResNet_v2_200, the improvement is again larger—1.42% in accuracy and 1.82% in fidelity.

Top-1 is not only slightly impacted by an oracle that only returns the top-5 predictions. For the rotation loss trained ResNet_v2_50 with 10% of the data, accuracy drops by 0.18%, and fidelity by 0.14%. For rotation loss trained ResNet_v2_200, accuracy drops by 1.19% and fidelity by 1.29%—this is still better than receiving the full prediction vector without using unlabeled data.

APPENDIX C PROTOTYPICALITY AND FIDELITY

We know from Section V that learning strategies struggle to achieve perfect fidelity due to the non-determinism inherent in learning. What remains to be understood is whether some samples are more difficult than others to achieve fidelity on. We investigate through the lens of recent work on identifying prototypical data points. Using each metric developed in Carlini *et al.* [43], we can rank the Fashion-MNIST test set in order of increasing prototypicality. Binning the prototypicality ranking into percentiles, we can measure how many models out of the 125 we trained for Section V agree on the same prediction. The intuition here is that more prototypical examples should be more consistently learnable, whereas more outlying points may be harder to consistently classify. Indeed, we find that this is the case - all metrics find a correlation between prototypicality and model agreement (fidelity), as seen in Figure 6. Interestingly, the metrics which do not use ensembles of models (adversarial distance and holdout-retraining) have the best correlation with the model agreement metric—roughly the top 50% of prototypical examples by these metrics are classified the same by nearly all 125 models.

Model	Fraction	ImageNet	WSL	WSL-5	ImageNet + Rot	WSL + Rot	WSL-5 + Rot
Resnet_v2_50	10%	(58.66/60.98)	(59.68/62.66)	(60.45/63.6)	(59.17/61.69)	(60.04/63.05)	(59.86/62.91)
Resnet_v2_200	10%	(61.17/63.81)	(63.05/66.40)	(62.79/66.36)	(62.52/65.04)	(64.47/68.22)	(63.28/66.93)
Resnet_v2_50	100%	(75.26/78.87)	(76.43/81.06)	(76.28/81.06)	N/A	N/A	N/A
Resnet_v2_200	100%	(77.56/81.19)	(78.57/83.91)	(78.24/83.2)	N/A	N/A	N/A

TABLE VIII

EXTRACTION ATTACK (TOP-1 ACCURACY/TOP-1 FIDELITY) OF THE WSL IMAGE NET MODEL BY MODEL AND SETTING. SEE TABLE II FOR INSTRUCTIONS ON READING THIS TABLE. WSL PROBABILITIES ALWAYS IMPROVE OVER IMAGE NET LABELS, EVEN WHEN ONLY THE TOP 5 PROBABILITIES ARE RETURNED. ROTATION PREDICTION LOSS DOES NOT SIGNIFICANTLY IMPROVE THE PERFORMANCE ON RESNET_v2_50, BUT PROVIDES A (1.42/1.82) IMPROVEMENT FOR RESNET_v2_200, WHICH IS ACTUALLY LARGER THAN THE PERFORMANCE BOOST GIVEN BY WSL LABELS ON 10% DATA. THERE IS STILL BENEFIT IN THE HIGH-DATA REGIME, WHERE WE OBSERVE A (1.17/2.19) IMPROVEMENT USING WSL LABELS.

Dataset	Metric	Algorithm	250 Queries	1000 Queries	4000 Queries
SVHN	Accuracy	Fully Supervised	79.25 \pm 0.89	89.47 \pm 0.28	94.25 \pm 0.16
SVHN	Accuracy	MixMatch	95.82 \pm 1.46	96.87 \pm 0.03	97.07 \pm 0.06
SVHN	Fidelity	Fully Supervised	79.48 \pm 0.87	89.87 \pm 0.25	94.71 \pm 0.18
SVHN	Fidelity	MixMatch	96.38 \pm 1.40	97.45 \pm 0.04	97.61 \pm 0.02
CIFAR10	Accuracy	Fully Supervised	53.35 \pm 0.19	73.47 \pm 0.14	86.51 \pm 0.08
CIFAR10	Accuracy	MixMatch	87.98 \pm 0.55	90.63 \pm 0.41	93.29 \pm 0.10
CIFAR10	Fidelity	Fully Supervised	53.61 \pm 0.17	73.96 \pm 0.11	87.37 \pm 0.09
CIFAR10	Fidelity	MixMatch	88.79 \pm 0.50	91.39 \pm 0.39	93.99 \pm 0.12

TABLE IX

EXTRACTION ATTACK PERFORMANCE OF FULLY SUPERVISED (FS) AND MIXMATCH (MM) EXTRACTION ON SVHN AND CIFAR10. THE SVHN ORACLE REACHES ACCURACY OF 97.36%, AND THE CIFAR10 ORACLE REACHES 95.75% ACCURACY. NOTE THAT THE BEST ACCURACY AND FIDELITY ACHIEVED BY MIXMATCH IS VERY CLOSE TO THE ORACLE’S PERFORMANCE FOR BOTH DATASETS. RESULTS ARE AVERAGED OVER 5 DIFFERENT SPLITS.

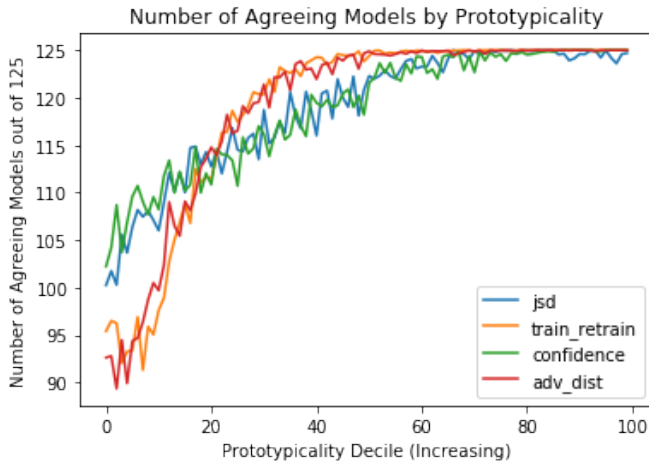


Fig. 6. It is easier to get fidelity on more prototypical examples. Using the 125 models we trained for understanding the impact of nondeterminism on fidelity, we counted the number of models which agree on the prediction made by their ensemble - the most predicted class. Then we bucket by percentiles in a prototypicality ranking, and plot the mean number of agreeing models. There is a positive correlation for every prototypicality metric considered, which is strongest for the adversarial distance and holdout retraining.

APPENDIX D SUPPLEMENTAL RESULTS FOR SECTION VI

In this section, we present supplemental results for Section VI. In Section VI, we measured the fidelity of our extracted model on test data and randomly augmented test data. Here, we provide two more metrics substantiating the fidelity of the technique.

Figure 7 shows a distribution over the bits of precision in the first weight matrix we extract on the 16-neuron neural

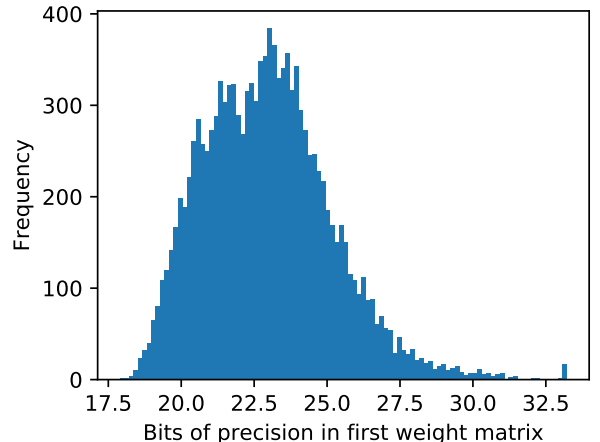


Fig. 7. For a 16-neuron MNIST model the attack works. The weights of the matrix are learned precisely. Plotted here is $\log_2 |W_{ij} - \hat{W}_{ij}|/|W_{ij}|$ where W is the true weight and \hat{W} is the learned weight.

network. All weights are identical in the first 17 bits, with the average identical on 23 bits.

Similarly, Figure 8 shows a distribution over the bits of precision in the difference between the logits (i.e., pre-softmax prediction) of the two networks. That is, formally, we measure the magnitude of the gap $|f_\theta(x) - f_{\hat{\theta}}(x)|$.

APPENDIX E QUERY COMPLEXITY OF FUNCTIONALLY EQUIVALENT EXTRACTION

In this section, we briefly analyze the query complexity of the attack presented in Section VI. We will assume that a

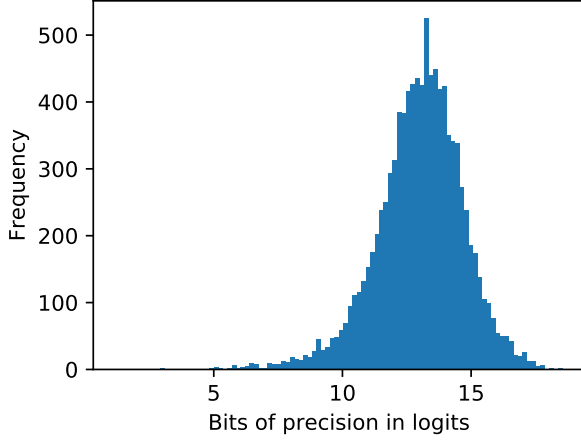


Fig. 8. For a 16-neuron MNIST model the attack works. Plotted here is number of bits of precision on the logits normalized by the value of the lot as done in the prior figure.

simulated partial derivative requires $O(1)$ queries using finite differences.

- 1) Critical Point Search. This step is the most nontrivial to analyze, but fortunately this was addressed in [19]. They found this step requires $O(h \log(h))$ gradient queries. We can simulate this with $O(h \log(h))$ model queries with finite differences.
- 2) Weight Recovery. This piece is significantly complicated by not having access to gradient queries. The absolute value recovery requires $O(d)$ queries per ReLU, weight sign recovery requires an additional $O(d)$, making this step take $O(dh)$ queries total.
- 3) Global Sign Recovery. For each ReLU, we require only three queries. Then this step is $O(h)$.
- 4) Last Layer Extraction. This step requires h queries to make the system of linear equations completely determined.

Overall, we find this algorithm requires $O(h \log(h) + dh + h)$. Because $d > h$, this is $O(dh)$. Extraction requires $\Omega(dh)$ queries without any auxillary information, as there are dh parameters. Then this algorithm is query-optimal up to a constant factor; this removes logarithmic factors that were present in Milli *et al.* [19].